forum acusticum 2026
8-12 September · Graz, Austria

INTEGRATING ACOUSTIC BLACK HOLES INTO SATELLITE ASSEMBLIES FOR VIBRATION REDUCTION

Jannik Krohn[1], Nikolai Kleinfeller[1], Heiko Atzrodt[1], Stephan Rapp[2], Eunjung Yoo[2]

[1] *Fraunhofer Institute for Structural Durability and System Reliability LBF, Bartningstr. 53, 64289 Darmstadt, Germany*

[2] *OHB System AG, Manfred-Fuchs-Straße 1, 82234 Wessling, Germany*

Abstract

In this work, Acoustic Black Holes (ABH) are integrated into an optical bench assembly (OBA) of a satellite, which is iso-statically mounted by three bipods to hold optical units with critical pointing stability requirements. A concept with a mass-neutral integration of a circular ABH in a second layer plate, as well as three lateral ABH strips around the circumference, is numerically analyzed to estimate the dynamic behavior and the potential of improvement. It is shown that vibrations are significantly reduced (by a maximum of approximately -14.4 dB) which is applicable to the effective microvibration attenuation. Additionally, ABHs can be used as tuned mass dampers (TMD) for challenging low-frequency in-plane and bending modes.

Keywords: *Aerospace, Satellite, Acoustic Black Hole*

1. Introduction

Spacecraft structures commonly having a high stiffness and a low mass making them very susceptible to vibrations [1]. Therefore, vibration isolation and vibration suppression systems are a difficult yet important task [2]. Vibration sources span the entire mission life, ranging from high-intensity transients in launch to environmental disturbances in-orbit [1, 2, 3]. In spacecraft, in-orbit microvibrations [1] usually occur from low frequency up to the kHz range. The aim is to reduce in-orbit microvibrations in spacecraft structures without adding additional mass. Vibration attenuation methods on spacecraft have been well documented [1] and have been seen to meet operational standards. Nevertheless, many approaches are plagued by drawbacks from the stringent requirements of space design, resulting in increased costs, complexity, and weight. Further, as space engineering advances, more payload is required to fulfill mission tasks, consequentially, more payload must be utilized and protected from the environment. This opens the door for a solution relatively simple and passive in nature, mechanically built-in to a structure, and potentially weight-saving, enter Acoustic Black Holes (ABH). An ABH is a local geometric taper with a near-zero-thickness tip within a host structure with a base thickness h_{host} [4, 5]. In this way, the propagation speed c_{B} of bending waves

$$c_{\mathrm{B}}(x) = \left[\frac{E \cdot \omega^2}{12\rho \cdot (1-\mu^2)}\right]^{\frac{1}{4}} \cdot \sqrt{h(x)}. \qquad (1)$$

is reduced, which depends, among other parameters like YOUNG's modulus E, the POISSON's ratio μ and the mass density ρ, on the thickness h of the host structure. If the thickness h is continuously reduced in a local region bounded by a und b, following a power-law [5]

$$h(x) = \begin{cases} h_{\mathrm{host}} \cdot \left(\frac{x-a}{b-a}\right)^m & \text{with } m \geq 2, a < x < b \\ h_{\mathrm{host}} & \text{if } x \geq b. \end{cases} \qquad (2)$$

the propagation speed c_{B} is reduced in the same manner. If the thickness h becomes zero, the bending wave is trapped and no reflection of the wave occurs at the edges. Since in a real-world application a thickness $h(a) = 0\,\mathrm{mm}$ can not be realized, damping material is attached in the region of largely reduced propagation speed c_{B}. Consequently, the wave is prevented from running out of the ABH again and is dissipated in a narrow region with only a small amount of damping material. The effect depends on the wavelength λ_{B}

Corresponding author: *Jannik.Krohn@lbf.fraunhofer.de.*

and is only given above a cut-on-frequency [5]

$$f_{\text{cut-on}} = \frac{h_{\text{host}}}{2\pi \cdot L_{\text{ABH}}^2} \cdot \sqrt{\frac{E \cdot (40 - 24\mu)}{12\rho \cdot (1 - \mu^2)}}. \qquad (3)$$

The theoretical length $L_{\text{ABH}} = (b - a)$ must be sufficiently large in order to achieve a low cut-on-frequency $f_{\text{cut-on}}$. ABH have been successfully tested in satellite applications as a vibration isolating system for sensitive electronics [6, 7]. In contrast, in this work, new concepts are developed for integrating ABH into an optical bench assembly (OBA) in order to reduce in-orbit microvibrations. This design approach achieves significant structural damping with minimal material usage compared to common measures.

2. Optical Bench Assembly

An exemplary OBA is designed as a host structure to evaluate the vibration reduction potential of the ABH within a realistic aerospace context (s. Fig. 1). An OBA serves as a mechanically decoupled connection for sensitive and fragile optical components in satellites and iso-statically mounted by three bipods. The core comprises a base plate, stiffening ribs, and threaded inserts. The base plate and ribs provide both global and local structural stiffness, while the inserts enable bolted connections for the attachment of optical components, the face sheet and the bipods. Here, all components are manufactured from aluminum (Al 6061-T6). This approach ensures a lightweight design with a total mass at approximately 26.35 kg without the dummy optical instruments (21.43 kg, represented by point masses in the numerical investigation, s. Fig. 9). The rib arrangement is optimized to ensure that

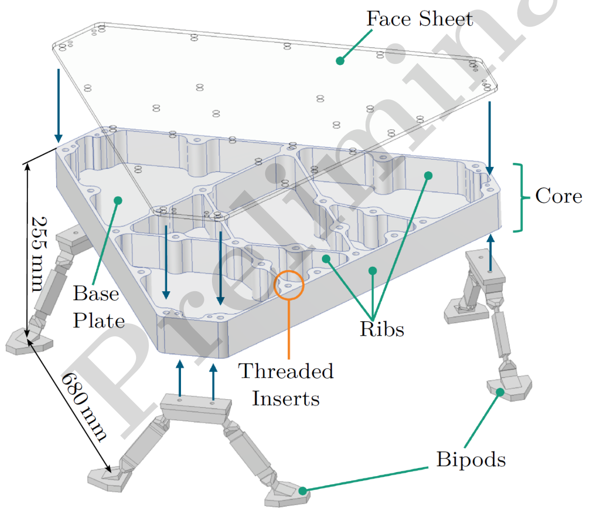

Figure 1: Design of the exemplary OBA without dummy optical instruments (face sheet is displayed transparently).

the global bending stiffness exceeds the effective shear stiffness contribution of the bipods. This results in a global bending mode frequency (s. Fig. 11 b) that is higher than the frequencies of the horizontal in-plane modes (s. Fig. 11 a). In addition, representative torsional and local bending modes occur at higher frequencies (s. Fig. 11 c–e). This dynamic behavior allows an assessment of the potential to reduce in-orbit microvibrations enabled by the integrated ABH.

3. Design and Integration of ABHs

The conceptual development phase involved evaluating the integration of various ABH configurations into the three primary components of the OBA: Bipods, core, and face sheet. The selection criteria focused on achieving low cut-on-frequency $f_{\text{cut-on}}$, therefore maximizing the ABH length, identifying the structural modes which interact with the ABH, preserving structural integrity, maintaining mass neutrality, and minimizing manufacturing complexity. The final design incorporates two ABH configurations (s. Fig. 2). First, a circular ABH is integrated into the base

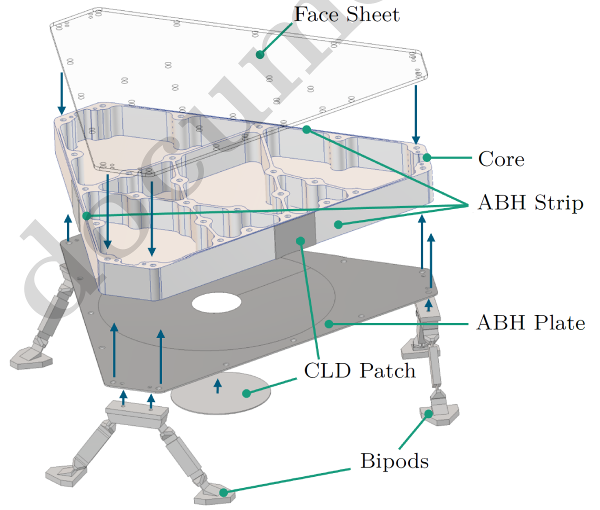

Figure 2: Design of the OBA with an integrated ABH plate and three lateral ABH strips.

plate of the core, therefore a second layer is created to maintain feasible manufacturing. By restricting the attachment between the second layer ABH plate and the base of the core to the threaded inserts on the outer edges, a large radius (r_{ABH}) and therefore a large effective ABH length is achieved, promising a low cut-on-frequency. To enhance flexibility, a hole (with radius r_{hole}) is introduced in the center of the ABH plate. A circular constrained layer damping (CLD) patch (with radius r_{CLD}) consisting of a viscoelastic elastomer layer (butyl, height h_{DL}) and a constraining aluminum layer (height h_{CL}) is applied over the hole and the edges of the ABH to maximize the high-strain region and thereby the energy dissipation. This configuration is primarily designed to reduce vertical initiated vibrations and additionally functions as a tuned mass damper (TMD) for the low-frequency global bending mode. Mass neutrality is maintained by reducing the wall thickness of the core base plate, while the second layer ABH plate still contributes to the global bending stiffness of the assembly. This ABH design is manufacturable with conventional milling processes. The integration into the OBA and the schematic representation of the ABH profile are shown in figure 3. The ABH profile (cross-section of the circular ABH) is defined by [8]

$$h_{\mathrm{plate}}(r) = h_{\mathrm{min}} + (h_{\mathrm{max}} - h_{\mathrm{min}}) \cdot \left(\frac{r}{r_{\mathrm{ABH}}}\right)^{m} \quad (4)$$

with the the minimum thickness

$$h_{\mathrm{min}} = \frac{\frac{h_{\mathrm{hole}}}{h_{\mathrm{max}}} - \left(\frac{h_{\mathrm{hole}}}{h_{\mathrm{max}}}\right)^{m}}{\frac{1}{h_{\mathrm{max}}} \cdot \left(1 - \frac{r_{\mathrm{hole}}}{r_{\mathrm{ABH}}}\right)^{m}}. \quad (5)$$

Detailed dimensions of the ABH and the CLD patch are provided in Table 1. Additionally, three lateral

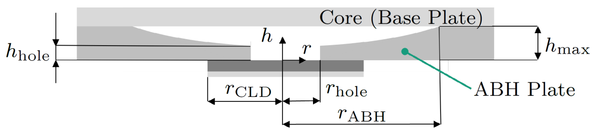

Figure 3: Schematic representation of the ABH plate (cross-section) with geometric dimensions.

Table 1: Design parameters of the ABH.

Parameter	ABH Plate	ABH Strip
m	3	2
h_{min}	–	1.2 mm
h_{max}	3 mm	4 mm
$r_{\mathrm{ABH}}/l_{\mathrm{ABH}}$	235 mm	300 mm
h_{hole}	1.75 mm	–
r_{hole}	50 mm	–
h_{DL}	2 mm	2 mm
h_{CL}	0.5 mm	0.5 mm
$r_{\mathrm{CLD}}/l_{\mathrm{CLD}}$	100 mm	100 mm
b	–	70 mm

ABH strips following the power law

$$h_{\mathrm{strip}}(x) = h_{\mathrm{min}} + (h_{\mathrm{max}} - h_{\mathrm{min}}) \cdot \left(\frac{x}{r_{\mathrm{ABH}}}\right)^{m} \quad (6)$$

are integrated into the outer ribs of the core (s. Fig. 2 and 4). These strips are designed to accommodate large ABH lengths (s. Tab. 1), specifically targeting horizontal initiated vibrations. Similar to the circular configuration, these strips serve as additional TMD for the low frequency in-plane modes. Mass neutrality is achieved by locally reducing the wall thickness of the outer ribs. This integrated ABH design is intended to contribute to the global bending stiffness of the core and to the local stiffness of the ribs to maintain the previous behavior. These ABH strips are embedded in the core and can be manufactured via wire electrical discharge machining (WEDM). The total mass of the OBA with the integrated ABHs is almost identical to the reference structure, excluding the mass of the CLD patches (0.157 kg).

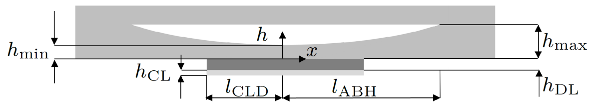

Figure 4: Schematic representation of one lateral ABH strip with geometric dimensions (with width b).

4. Numerical Investigation

The numerical investigation of the OBA, incorporating ABH features, is conducted using the finite element analysis (FEA) software Ansys Workbench 2025 R1. To characterize the dynamic behavior of the assembly, modal analyzes are performed and coupled with harmonic analyzes within the Ansys Mechanical environment. The material properties are modeled as isotropic and linear elastic. Aluminum components are defined based on standard material data provided by the Ansys material library. For the butyl damping material, properties are determined experimentally in previous projects (s. Tab. 2) and show similarities to those reported by Hoffmann et al. [8]. The modal analysis is performed on the undamped structure within a frequency range up to 1500 Hz. For the harmonic analysis, a modal superposition method is used covering a frequency range up to 1000 Hz. Consistent with empirical data from OHB, a global critical damping ratio of $D = 0.5\,\%$ is applied to the model. All structural interfaces are modeled using bonded contact conditions. FE with second-order shape functions and sufficiently small element sizes are utilized throughout the model to ensure computational accuracy. The core structure (element size 20 mm), including the ABH strips (5 mm), bipods (10 mm), and the face sheet (10 mm), is discretized using 10-node tetrahedral elements (SOLID187). The ABH plate (2 mm) and the aluminum layers of the CLD patches (3 mm) are modeled using 8-node square shell elements (SHELL281). The CLD patches are represented by 3 mm 20-node hexahedral solid elements (SOLID186).

The shape of the ABH, within the ABH plate, is generated by a varying element thickness $h_{plate}(r)$ (s. Fig. 5) via an APDL script. Therefore, a radially symmetric mesh composed of square shell elements is needed. For each element, the radial distance to a coordinate system, located at the center of the ABH, is calculated. The thickness of the element h_i is then determined with equation 4 and 5 based on this distance r_i. Afterwards an offset is applied corresponding to half of the element thickness. The accuracy of the ABH shape is direct correlated with the refinement of the mesh. Therefore, a small element size is needed.

Prior to the integration into the full assembly, individual ABH components are simulated to evaluate their damping effectiveness and to optimize the integrated TMD effect towards a target resonance. This investigation is demonstrated using the ABH plate. For

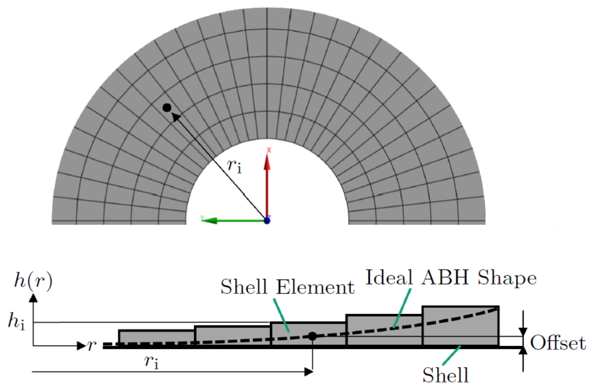

Figure 5: Generating an ABH shape with varying thickness of shell elements.

Table 2: Material parameters of the structure and the damping layer.

Parameter	Aluminum	Butyl
mass density ρ	$2770\,\mathrm{kg/m^3}$	$1500\,\mathrm{kg/m^3}$
YOUNG's modulus E	71000 MPa	1.2 MPa
POISSON's ratio μ	0.33	0.42
loss factor η	–	1
RAYLEIGH damping α	0.256	–
RAYLEIGH damping β	$4.62{\cdot}10^{-7}$	–

the modal analysis, the plate is constrained at the 15 mounting holes (s. Fig. 6). To achieve this, all degrees of freedom (DOF) of a central node located beneath the plate is fixed and these constraints are transferred to the mounting holes via a Rigid Body Element (RBE). In the harmonic analysis, an acceleration of $1\,\mathrm{m\,s^{-2}}$ is applied in the vertical direction (z-axis) through this central node (utilizing 500 solution intervals with 2 Hz frequency steps). The investigation compares four configurations: A reference plate (without a ABH) with (3.08 kg) and without CLD patches (2.94 kg) and the ABH plate with (2.7 kg) and without CLD patches (2.56 kg).

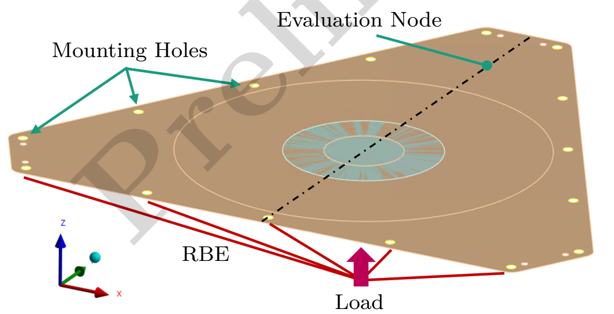

Figure 6: FE-Model of the single ABH plate with boundary conditions (without visualizing the finite elements).

The results are evaluated by analyzing the frequency response function (identical to the acceleration amplitude, s. Fig. 7) at an evaluation node located outside the ABH region (s. Fig. 6), as well as by examining the mode shapes at concise resonances (s. Fig. 8). The reference plate without ABH exhibits the highest acceleration peaks, which are slightly damped by the application of CLD patches. Concurrently, the resonance frequencies shift downward due to the additional mass of the CLD material. The ABH plate, due to its reduced structural stiffness, shows an increase of the amplitudes compared to the reference plate with CLD, followed by a further reduction of the resonance frequencies. Significant damping and a substantial reduction in amplitude, while reducing the overall mass, is only achieved when the ABH is combined with a CLD patch (s. Fig. 7). Despite the integration of the ABH, resonances still occur, and a distinct cut-on-frequency is not immediately apparent. Strong damping effects appear to emerge only at higher frequencies (> 800 Hz), suggesting the cut-on-frequency in this range.

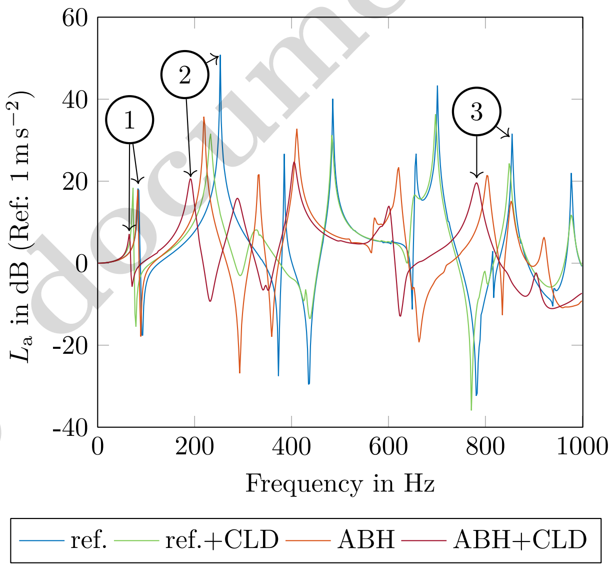

Figure 7: Acceleration level L_a at evaluation node for the single ABH plate.

This observation is supported by the comparison of mode shapes, where the total deformation (in mm) increasingly concentrates in the center of the ABH as the frequency rises (s. Fig. 8). The second bending mode of the ABH plate at 192 Hz is specifically tuned to be near at the frequency of the global bending mode of the reference OBA (at 188 Hz), allowing the ABH to function as a TMD for low-frequency excitation. To achieve the required stiffness, the geometry of ABH is varied specifically by the power-law exponent m and the minimum thickness at the edge of the hole h_{hole}. The first mode was intentionally avoided for this tuning, as it would require significantly higher stiffness, thereby increasing the cut-on-frequency. Consequently, a design balance must be found, utilizing a higher-order bending mode as a TMD while maintaining low structural stiffness to achieve the lowest possible cut-on-frequency. This optimization strategy is also applied to the lateral ABH strips to effectively

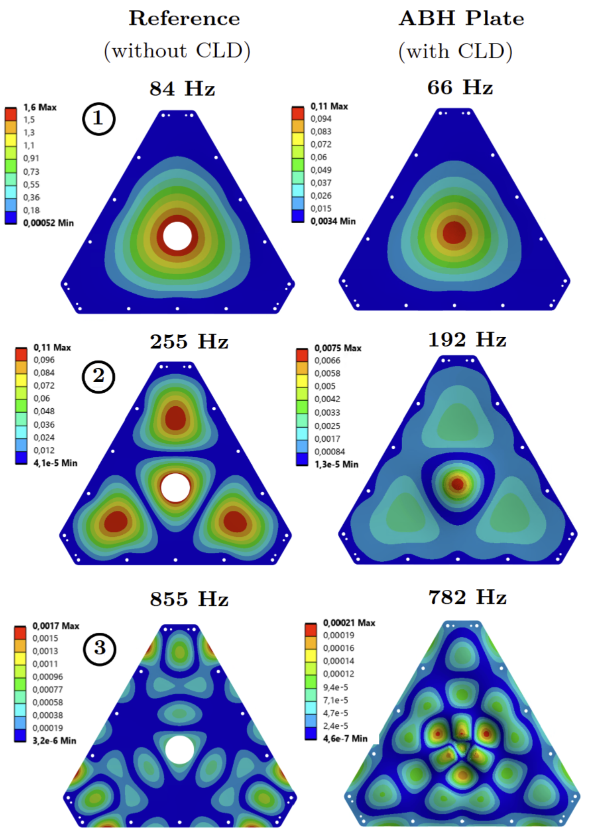

Figure 8: Mode shapes at concise resonances visualized by the global displacement in mm (the CLD patch covers the hole in the center of the ABH plate).

reduce horizontal in-plane vibrations of the OBA. The numerical analysis of the full OBA follows the methodology established for the component simulation. The setup utilizes identical analysis parameters with an increased frequency resolution of 1000 solution intervals (1 Hz steps). The dummy optical instruments are positioned according to OHB specifications and are modeled as point masses. Structural excitation is applied via a central node, coupled to the feet of the bipods through RBEs. For modal analysis, all DOFs at the central node are constrained, while the harmonic analysis employs a base acceleration of $1\,\mathrm{m\,s^{-2}}$ in x, y and z-direction (s. Fig. 9).

For the evaluation, the mean acceleration amplitudes of the point masses and their resulting vector are determined (s. Fig. 10). The results demonstrate that the ABHs effectively function as TMDs for both in-plane and global bending modes, evidenced by the characteristic peak splitting and the emergence of antiresonances. This TMD effect results in a significant amplitude reductions by approximately -11.0 dB at 160 Hz (in-plane mode) and -14.4 dB at 190 Hz (global bending mode). Further reduction of the amplitude due to damping is observed at higher resonances, including -0.7 dB at 300 Hz and -5.8 dB at 400 Hz (torsional modes), as well as -8.9 dB at 700 Hz (local bending). Analyzing the mode shapes visualizes

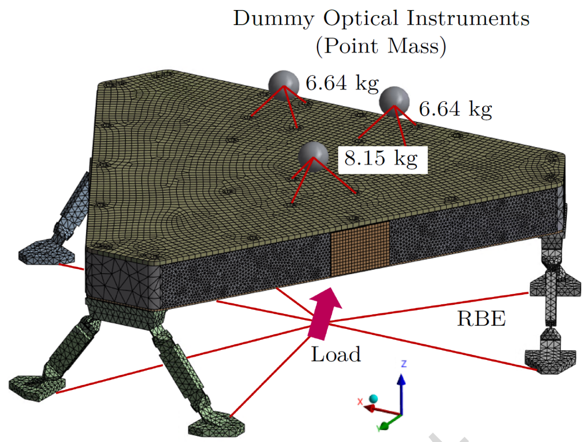

Figure 9: FE-Model of the OBA with integrated ABHs and boundary conditions.

that the ABH plate is the primary source of damping, as deformations increasingly concentrate in the ABH center at higher frequencies (s. Fig. 11). While the lateral ABH strips successfully reduce global in-plane vibrations by operating in their second bending mode as a TMD, their contribution to damping at higher frequencies remains limited. The higher-order bending mode of the ABH plate effectively counteract the global bending of the OBA.

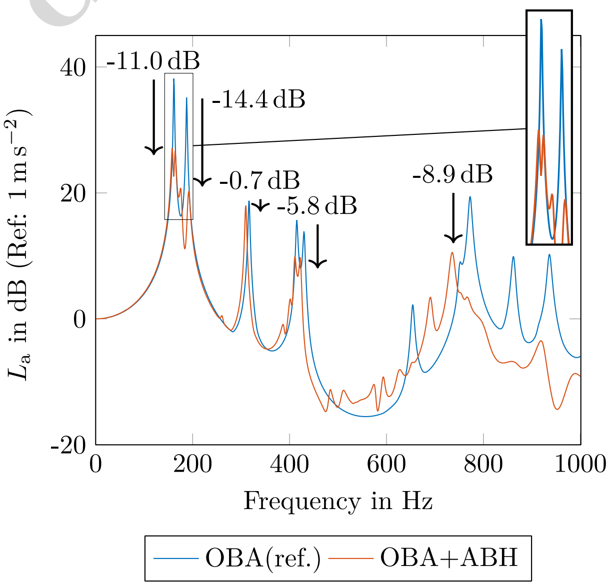

Figure 10: Acceleration level L_a at dummy masses.

In summary, the ABH integration provides a mass-neutral strategy for significant vibration reduction. The damping of the ABH can be used effectively in a complex assembly across a broad frequency range, with particularly strong dissipation above 800 Hz, likely indicating the cut-on-frequency $f_{\mathrm{cut-on}}$. Furthermore, the results confirm that ABHs are also suitable for highly integrated TMDs, to address specific low-frequency resonances below the cut-on-frequency.

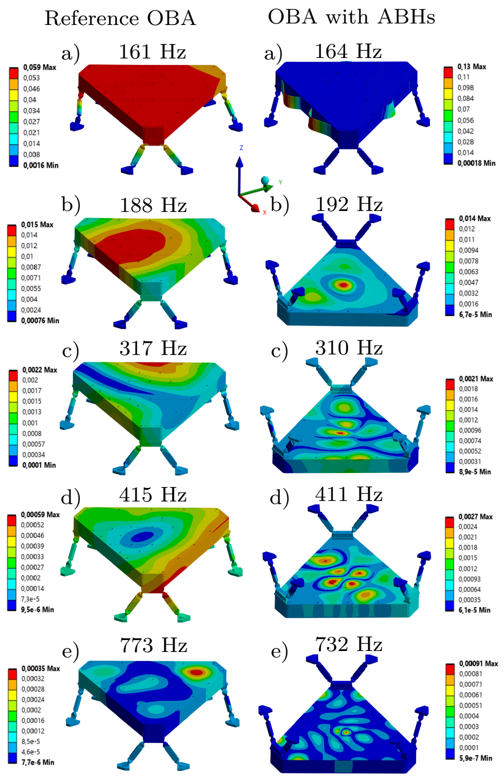

Figure 11: Comparing the mode shapes of the reference and the OBA with ABHs at concise resonances visualized by the global displacement in mm (scaling factor: 500).

The design process necessitates a careful balance between utilizing higher-order modes for a targeted absorption and maintaining low structural stiffness to ensure a wide range of damping effectiveness.

5. Conclusion

This work demonstrates the design potential of ABH for improving the vibroacoustic properties of complex mechanical structures, using an optical bench assembly (OBA) of a satellite as an aerospace example. The main advantage of the ABH lies in its integration into the existing structure without requiring additional space or adding to its basic mass. It is shown that two key effects of an ABH can be utilized by a proper design to reduce in-orbit microvibrations. First, the ABH can be used as a TMD to tackle low-frequency resonances. Second, the ABH effect is utilized to dampen in-orbit microvibrations in the higher frequency range. The findings make a significant contribution to the design of ABHs for complex mechanical systems. In the future, potential improvements to the existing design will be investigated. This includes a better tuning of the absorbing effect of the ABH and an increased damping effectiveness by adjusting the position of the CLD patches. In addition, a down-scaled technology demonstrator is being built to experimentally validate the numerical simulation and investigate aspects related to the manufacturing.

6. Acknowledgments

This work is funded by the Federal Ministry of Research, Technology and Space BMFTR in Germany (Grant number 50RP2595A).

With funding from the:

Federal Ministry
of Research, Technology
and Space

References

[1] W. Xing, W. Tuo, X. Li, T. Wang, and C. Yang, "Micro-vibration suppression and compensation techniques for in-orbit satellite: A review," *Chinese Journal of Aeronautics*, vol. 37, no. 9, Jan. 2024. DOI: 10.1016/j.cja.2024.05.036.

[2] X. Jiao, J. Zhang, W. Li, Y. Wang, W. Ma, and Y. Zhao, "Advances in spacecraft micro-vibration suppression methods," *Progress in Aerospace Sciences*, vol. 138, Mar. 2023. DOI: 10.1016/j.paerosci.2023.100898.

[3] L. Li et al., "Micro-vibration suppression methods and key technologies for high-precision space optical instruments," *Acta Astronautica*, vol. 180, Mar. 2021. DOI: 10.1016/j.actaastro.2020.12.054.

[4] A. Pelat, F. Gautier, S. C. Conlon, and F. Semperlotti, "The acoustic black hole: A review of theory and applications," *Journal of Sound and Vibration*, vol. 476, Mar. 2020. DOI: 10.1016/j.jsv.2020.115316.

[5] O. Aklouche, A. Pelat, S. Maugeais, and F. Gautier, "Scattering of flexural waves by a pit of quadratic profile inserted in an infinite thin plate," *Journal of Sound and Vibration*, vol. 275, May 2016. DOI: 10.1016/j.jsv.2016.04.034.

[6] X. Lyu, H. Sheng, M. He, Q. Ding, L. Tang, and T. Yang, "Satellite vibration isolation using periodic acoustic black holes structures with ultrawide bandgap," *Journal of Vibration and Acoustics ASME*, vol. 145, Aug. 2022. DOI: 10.1115/1.4054978.

[7] J. H. Jun and J. S. Lee, "Effective mitigation of impulsive vibration in satellite electronic units using acoustic black hole structure," *Applied Acoustics*, vol. 225, Jul. 2024. DOI: 10.1016/j.apacoust.2024.110165.

[8] S. Hoffmann, S. Rothe, and S. C. Langer, "Acoustic black holes – modelling, shaping, placement and application," in *Calm, Smooth and Smart: Novel Approaches for Influencing Vibrations by Means of Deliberately Introduced Dissipation*, Springer, 2023, pp. 169–188. DOI: 10.1007/978-3-031-36143-2_9.